Comparing theoretical demagnetizing factors with the observed saturation process in rectangular shields

Amikam Aharoni, Ladislav Pust, and Mark Kief

Citation: Journal of Applied Physics **87**, 6564 (2000); doi: 10.1063/1.372771
View online: http://dx.doi.org/10.1063/1.372771
View Table of Contents: http://scitation.aip.org/content/aip/journal/jap/87/9?ver=pdfcov
Published by the AIP Publishing

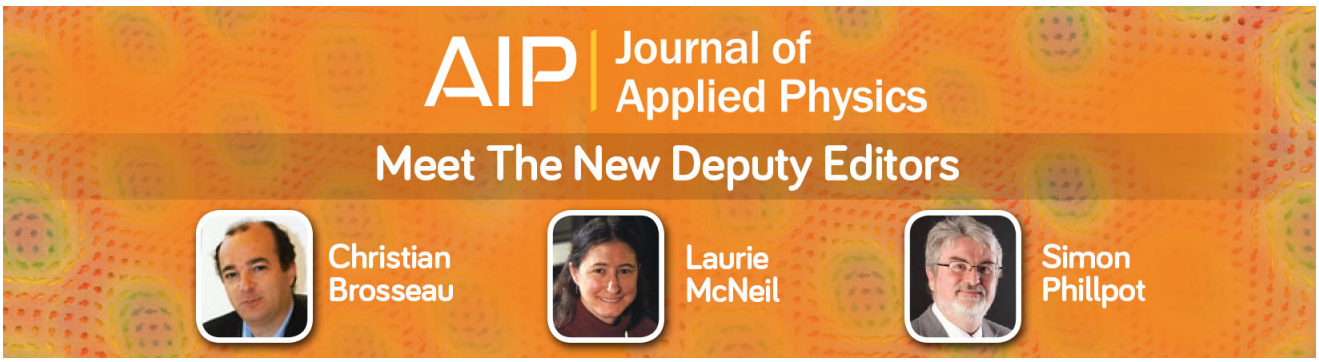

Comparing theoretical demagnetizing factors with the observed saturation process in rectangular shields

Amikam Aharoni[a)]
Department of Electronics, Weizmann Institute of Science, 76100 Rehovoth, Israel

Ladislav Pust[b)] and Mark Kief
Seagate Technology, Bloomington, Minnesota 55435-5489

An analytic expression is given for the ballistic demagnetizing factors, D', of the general rectangular prism, in which the field is averaged over the middle cross section of the prism, and for the ''side'' demagnetizing factor, D'', in which the averaging is over the edges of the prism. The demagnetizing fields are compared with the applied field values when a $250\times 95\times 2.35\,\mu$m magnetic shield transfers into the saturated state. This shield was made of a Ni_{80} Fe_{20} film, with a small uniaxial magnetic anisotropy induced during the electroplating process. Domain structure and the process of magnetic saturation were imaged using wide-field Kerr microscopy in fields up to 400 Oe, both along the easy and the hard axes. The ballistic demagnetizing field is found to be close to the external field necessary to align magnetically the central part of the shield, while the full shield saturation takes place at a field above the recently published magnetometric demagnetizing field. Saturation fields along the hard uniaxial anisotropy axis are larger, due to effective anisotropy fields.
 [S0021-8979(00)20108-4]

I. INTRODUCTION

Demagnetizing fields in a rectangular ferromagnetic prism are nonuniform even if the prism is magnetically saturated. This field varies significantly along the prism, being the largest at the edges with magnetic charge and the smallest in the center. Therefore, the recently published[1] analytical expression for the *magnetometric* demagnetizing factor D, namely, the factor obtained by averaging the field over the entire prism, does not yield the range of demagnetizing fields. This does not reveal how low the local demagnetizing field is in the central part of the prism, and how high it is at the edges where the magnetic charges are. Here, we give an analytic expression for the *ballistic* demagnetizing factor D', defined as the average over the central cross section of the prism, where the demagnetizing field is the lowest, so that D' is inherently smaller than D. We also give an analytic expression for the ''side'' demagnetizing factor D'', defined as the average over the charged edges of the prism, where the demagnetizing field is the highest.

In the calculation of D, D', and D'', the prism is assumed to be uniformly magnetized, which is the case only under a very large external magnetic field, H_{appl}. Otherwise, a domain structure is present, with a complex distribution of the magnetic charge. In Sec. III, we compare these theoretical values with the real demagnetization in an actual domain structure in ferromagnetic prisms.

II. THEORY

We consider a uniform and homogeneous ferromagnetic rectangular prism, defining the origin of a Cartesian coordinate system at the center of this prism. Specifically, we take the prism (as in Refs. 1 and 2) to extend over the volume $-a\leqslant x\leqslant a$, $-b\leqslant y\leqslant b$ and $-c\leqslant z\leqslant c$, see also Fig. 1 in Ref. 1. If this prism is saturated by a field H_{appl} along z, a surface charge is created on its faces $z=\pm c$. The potential due to this charge is given by well-known integrals on these surfaces, and the magnetic field is the gradient of that potential. The average of this field over the prism volume yields the *magnetometric* demagnetizing factors.[1] Here we consider the *ballistic* demagnetizing factor in the z direction, D'_z, defined by Brown[3] as the component of the tensor D' in the relation

$$\langle H\rangle_{\text{av}}=H_{\text{appl}}-H'_d=H_{\text{appl}}-4\pi D' M_{\text{s}}, \tag{1}$$

where H_{appl} is the applied field, M_{s} is the saturation magnetization, and H'_d is the local demagnetizing field averaged over the middle cross section, namely, an average over x and y for $z=0$. We also define the ''side'' demagnetizing factor D''_z and the ''side'' demagnetizing field H''_d by the same relation as in Eq. (1), for the same averaging at $z=\pm c$ instead of $z=0$.

The integrations involved in this averaging are similar to those evaluated in Ref. 1, and have been carried out in a similar way, leading to

$$\begin{aligned}\pi D'_z=&\frac{c}{2a}\ln\left(\frac{\sqrt{4a^2+4b^2+c^2}+2b}{\sqrt{4a^2+4b^2+c^2}-2b}\times\frac{\sqrt{4b^2+c^2}-2b}{\sqrt{4b^2+c^2}+2b}\right)\\&+\frac{c}{2b}\ln\left(\frac{\sqrt{4a^2+4b^2+c^2}+2a}{\sqrt{4a^2+4b^2+c^2}-2a}\right.\\&\left.\times\frac{\sqrt{4a^2+c^2}-2a}{\sqrt{4a^2+c^2}+2a}\right)+\frac{c}{2ab}(\sqrt{4a^2+c^2}\\&+\sqrt{4b^2+c^2}-\sqrt{4a^2+4b^2+c^2}-c)\\&+2\arctan\left(\frac{4ab}{c\sqrt{4a^2+4b^2+c^2}}\right).\end{aligned} \tag{2}$$

a)Electronic mail: a.aharoni@ieee.org
b)Electronic mail: lpust@notes.seagate.com

In the particular case $b\to\infty$, by using the notation

$$p=\frac{c}{a}, \tag{3}$$

Eq. (2) reduces to the equation published[3] by Brown,

$$\pi D_z'=2\arctan\left(\frac{2}{p}\right)-\frac{p}{2}\ln\left(1+\frac{4}{p^2}\right). \tag{4}$$

In the particular case of a square cross section, $a=b$, the use of the notation of Eq. (3) in Eq. (2) leads to

$$\pi D_z'=p\ln\left(\frac{\sqrt{p^2+8}+2}{\sqrt{p^2+8}-2}\times\frac{\sqrt{p^2+4}-2}{\sqrt{p^2+4}+2}\right)+2\arctan\left(\frac{4}{p\sqrt{p^2+8}}\right)+p\left(\sqrt{p^2+4}-\frac{\sqrt{p^2+8}+p}{2}\right). \tag{5}$$

The particular case considered in Ref. 4, $b=2a$, can also be obtained directly from Eq. (2). With the notation of Eq. (3), it is

$$\pi D_z'=\frac{p}{2}\ln\left(\frac{\sqrt{p^2+20}+4}{\sqrt{p^2+20}-4}\times\frac{\sqrt{p^2+16}-4}{\sqrt{p^2+16}+4}\right)+\frac{p}{4}\ln\left(\frac{\sqrt{p^2+20}+2}{\sqrt{p^2+20}-2}\times\frac{\sqrt{p^2+4}-2}{\sqrt{p^2+4}+2}\right)+2\arctan\left(\frac{8}{p\sqrt{p^2+20}}\right)+\frac{p}{4}(\sqrt{p^2+4}+\sqrt{p^2+16}-\sqrt{p^2+20}-p). \tag{6}$$

All these expressions are for the demagnetizing factor D' (i.e., also the demagnetizing field H_d') in the central region of the prism, where the fields are relatively small. Similar averaging over the regions with the highest demagnetizing field, i.e., at $z=\pm c$, leads to

$$\pi D_z''=\frac{c}{2a}\ln\left(\frac{\sqrt{a^2+b^2+c^2}+b}{\sqrt{a^2+b^2+c^2}-b}\times\frac{\sqrt{b^2+c^2}-b}{\sqrt{b^2+c^2}+b}\right)+\frac{c}{2b}\ln\left(\frac{\sqrt{a^2+b^2+c^2}+a}{\sqrt{a^2+b^2+c^2}-a}\times\frac{\sqrt{a^2+c^2}-a}{\sqrt{a^2+c^2}+a}\right)+\frac{c}{ab}(\sqrt{a^2+c^2}+\sqrt{b^2+c^2}-\sqrt{a^2+b^2+c^2}-c)+\frac{\pi}{2}+\arctan\left(\frac{ab}{c\sqrt{a^2+b^2+c^2}}\right). \tag{7}$$

It is seen from Eq. (7) that $D_z''\to 1$ for $c\to 0$, namely, for a thin prism magnetized perpendicular to the film plane. For $a\to 0$, namely, for the field applied in the plane, $D_z''\to\frac{1}{2}$.

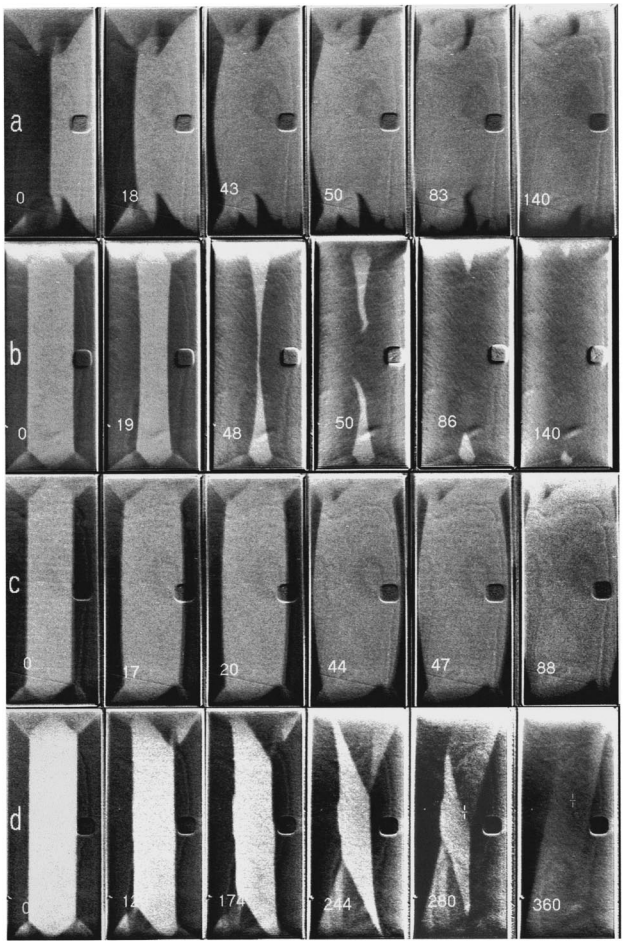

FIG. 1. Kerr images of the domain structure in a prism $250\times 95\times 2.35$ μm made of Ni_{80} Fe_{20} film. The small square on the right-hand side is a nonmagnetic feature on the surface that does not affect the magnetic behavior. The labels are the values of H_{appl} in Oersted. In (a), (b), and (c), H_{appl} is along the long axis, while it is along the short axis in *d*. This field, H_{appl}, is antiparallel in (b), parallel in (c), and perpendicular in (d) to the center domain.

III. EXPERIMENT

A 2.35 μm thick $Ni_{80}Fe_{20}$ film ($4\pi M_s=10\,000$ G), with a uniaxial magnetic anisotropy, $H_k\approx 2$ Oe, induced during the electroplating process, was patterned into rectangular magnetic shields with various dimensions. In this article we present results obtained on a shield 250×95 μm. Other data will be published elsewhere. Domain structure and the process of magnetic saturation were imaged using the wide-field Kerr microscopy in fields up to 400 Oe, along both the easy and the hard axes. In addition, the local magnetic field was later measured by a small giant magneto resistance (GMR) sensor, attached at the center.

The theoretical demagnetizing factors of this shield are $D_z'=0.0020$ and 0.0130, and $D_z=0.0141$ and 0.0382, respectively, for H_{appl} along the long and the short axis. The corresponding demagnetizing fields in Oe are obtained, according to Eq. (1), by multiplying each of these numbers by 10^4. $D_z''\approx 0.5$ for both field directions.

Figure 1 shows how domain structures change with H_{appl} applied parallel to the shield plane, both along the long [Figs. 1(a)–1(c)] and the short [Fig. 1(d)] axis. By a suitable field

history, we can generate a starting zero-field domain structure consisting of one, two, three, or more domain walls along the long axis. In 1(b), H_{appl} is antiparallel, and in 1(c), it is parallel to the center domain. At $H_{\text{appl}} \approx H'_{\text{d}} = 20$ Oe, the domain structure is similar to that at zero-field, with all the domain walls going through the whole shield. There is a quantitative change in the domain structure when the two domain walls annihilate, at about 47 Oe. The sensor at the center of the shield shows the local field to be nearly zero for $H_{\text{appl}} < 47$ Oe, with a sharp onset of a local field at higher $H_{\text{appl}} > 47$ Oe. At higher fields, there are no domain walls in the central region, but there are traces of domains near the shield edges even at larger fields than the magnetometric demagnetizing field $H_d = 141$ Oe.

A similar scenario is observed for H_{appl} parallel to the center domain [Fig. 1(c)], except that domain walls merge at $H_{\text{appl}} \approx 47$ Oe into the edges of the shield. The structural change was similar when we started from other zero-field configurations, such as the single longitudinal wall in Fig. 1(a), or when we used another shield size.

At $H_{\text{appl}} = H_d = 141$ Oe, most of the shield is saturated, which means that H_{appl} is larger than the local demagnetizing field in this region. The saturated region, however, cannot extend all the way to the shield charged edges if H_{appl} is smaller than the ballistic demagnetizing field averaged over these edges, $H''_d \approx 5000$ Oe. Therefore, traces of domain structure adjacent to these edges are observed even at fields above H_d.

The magnetization process was also observed for in-plane fields applied parallel to the short axis of the prism, namely, along the anisotropy hard axis. The demagnetizing fields in this case are $H_d = 382$ Oe and $H'_d = 130$ Oe. The images shown in Fig. 1(d) for this case suggest a process similar to the easy axis case, where the domains with magnetization along the applied field grow at the expense of the oppositely oriented domains. The GMR sensor indicates an onset of a local field at about 225 Oe. Again, H_d tends to underestimate, and H''_d tends to overestimate, the observed field needed to achieve a ''local'' saturation in the center of the magnetic shield.

We can thus relate the analytic expressions for the demagnetizing factors and fields with the magnetic behavior of real prisms at finite fields, even though the former were obtained by assuming a uniform magnetization, with the magnetic charges localized on the prism edges.

The Kerr images and field sensor measurement data indicate that when applying H_{appl}, the magnetic domain structure changes in such a way that low applied fields are effectively canceled by the demagnetizing field. Inspection of the magnetic domain structure at low fields indicates that the internal domain walls must be charged. It means that not all the magnetic charges are on the prism edges, as assumed in the calculation. This field cancellation process can continue as long as there is a domain structure to change. After domain walls either annihilate each other [as in Fig. 1(b)], or disappear into edges of the sample [as in Figs. 1(a) and 1(c)], H_{appl} cannot be compensated by the demagnetizing field any more, and indeed the local field sensor shows a sharp onset of a local field. As seen in Figs. 1(a)–1(c), there is also no domain structure in the central region at fields above 47 Oe.

IV. CONCLUSIONS

The demagnetizing fields H_d, H'_d, and H''_d, evaluated respectively from the demagnetizing factors D_z, D'_z, and D''_z using Eq. (1), characterize the magnetic behavior of a prism even at the low-field state, in which the shield is multidomain. The ballistic demagnetizing field H'_d evaluated from Eq. (2) is a lower bound for the field necessary to saturate the prism in the central part. For prism dimensions studied in this article H'_d is about half of the field necessary to saturate the central part of the prism.

The magnetometric demagnetizing field H_d evaluated in Ref. 1 gives the field at which a significant part of the prism is saturated, except for a small area near the charged edges, where traces of domains can be observed even in fields well above H_d.

The ''side'' demagnetizing field H''_d is essentially the highest local demagnetizing field existing in the magnetically saturated shield. It means that in a perfect material with an ideal shape, at $H_{\text{appl}} > H''_d$ there should be no trace of domain structure left in the prism.

[1] A. Aharoni, J. Appl. Phys. **83**, 3432 (1998).
[2] R. I. Joseph and E. Schlömann, J. Appl. Phys. **36**, 1579 (1965).
[3] W. F. Brown, Jr., *Magnetostatic Principles in Ferromagnetism* (North-Holland, Amsterdam, 1962), Appendix.
[4] G. Zheng, M. Pardavi-Horvath, X. Huang, B. Keszei, and J. Vandlik, J. Appl. Phys. **79**, 5742 (1996).